A review of our recent work on Raman scattering and a tribute to K. S. Krishnan

S. C. Jain

IMEC, Kapeldreef 75, 3001 Leuven, Belgium

Raman scattering was discovered in India by Raman and Krishnan in 1928. After 70 years of the discovery, there is still an intense activity in this field world wide. Though a large body of experimental and theoretical work exists on the subject, there are many experimental situations where it is difficult to interpret the observed Raman spectra. One such example is the Raman scattering from in-homogeneously strained semiconductors. In modern integrated circuit chips and heterostructure devices, the stress varies on a length scale of a few nanometers. Typically, diameter of a focused laser beam is ~ 1 μm and penetration depth can vary from a few microns to several millimeters. The laser beam samples a large volume of the strained structure. Each point in this volume scatters light with a Raman frequency characteristic of stress at that point. Because the beam is usually focused, the distribution of light intensity in this volume is very complex. The interpretation of observed Raman spectra is therefore very difficult. Recently we have developed a method to calculate theoretically the Raman spectra from such structures. We used Finite Element Method to calculate the stress and strain tensors. We solved the secular equation numerically to obtain Raman frequencies as a function of stress components. We constructed an expression for the distribution of intensity of light inside the semiconductor taking into account the depth at which the beam is focused. We calculated spectra from closely spaced points in the volume sampled by the laser light. We then superposed all these spectra to obtain the spectrum that will be observed in an experiment. Contrary to the usual belief that light penetrates only up to a depth = $1/\alpha$ (where α is the absorption coefficient), we found that the light scattered from much larger depths modifies the Raman spectrum. The calculated spectra agree with the observed spectra from quantum wires, from structures used in local oxidation of Si needed for fabricating IC chips and from other heterostructure devices. A brief review of this work is given in this paper.

Preliminary remarks, my association with K. S. Krishnan

Raman scattering was discovered by Raman and Krishnan[1] in Calcutta in 1928. The number of research groups who have studied Raman scattering runs into hundreds of thousands. I searched INSPEC for journal papers published on Raman scattering during the period 1980 to 1997. The number came out to be 54980! This number does not include numerous conference papers, book chapters and books published on Raman scattering. Scientists and engineers working in almost all scientific disciplines have contributed to the study of Raman scattering. Raman scattering has found applications not only in physics and chemistry but also in medicine, civil engineering, electrical engineering, mechanical engineering and numerous other fields. We have been interested in studying Raman scattering in semiconductors and devices. The recent work done by me with a number of my collaborators is described in this review. The names of the collaborators can be found from the list of papers quoted in the list of references given at the end of this review.

This review has been prepared to honour late Krishnan on the occasion of his birth centenary. After publishing the first paper on Raman scattering, Krishnan moved to other fields and later, Raman was awarded the Nobel prize for the discovery. I have chosen this subject partly because Krishnan was a co-author of the first paper in which the discovery was reported and partly because this is the only field in which I have been involved in recent years.

I wrote in the Preface of my recent book[2], 'I must express my gratitude to the late K. S. Krishnan, F.R.S., who taught me techniques of investigations'. I worked with Krishnan closely for more than 10 years. We published extensively on many different topics in physics. In fact I worked with him until the day he died. On this fateful day, I was in Mussorie attending a Summer School. I received a telephone call from his secretary asking me to come to Delhi so that we (Krishnan and I) could make corrections to a paper which was to be published in *Nature*. We sat in his office until about 9 pm, we finished the corrections and he signed the letter forwarding the paper to *Nature*. He gave me a ride to my home in his private car. After a few hours

he died. It made many of us very sad for a long time. He was not only a great physicist and a great scholar, he was a great human being. I am greatly honoured by this invitation to write a paper for the volume being published to honour the great man, Krishnan.

Raman scattering from inhomogeneously strained structures

Semiconductor devices and integrated circuit (IC) chips contain overlayers and buried elements of materials different from that of the substrate[2-5]. Stresses in the heterostructures are generated due to mismatch in the coefficients of thermal expansion and in the lattice constants of the film or the buried element and the substrate[3]. In 1970, LOCOS (LOCal Oxidation of Silicon: a processing technique for isolation) was invented. The LOCOS structure consists of a composite stripe of nitride/polysilicon on a Si substrate. This structure gives rise to stripe edge-induced stresses in the substrate which generate harmful dislocations. In late 1970s and 1980s several studies of stresses induced in LOCOS structures or in structures containing isolation trenches were made. An excellent review of the early work has been written by Hu[3] in 1991. More recent work is described in references[4,6,7].

As the size of devices on the IC chip started decreasing to very small dimensions, the problem created by the stresses generated in the chip became more serious. The stripe width in LOCOS structures decreased to 2 to 5 microns[8-10]. Hu's analytical theory (see the review[3] for references) of edge-induced stresses in the substrates worked reasonably well with wider stripes but gave erroneous results for narrow stripes. Analytical methods were not able to give accurate values of the stress distribution. It became necessary to use Finite Element (FE) method to calculate these stresses[11]. At the same time micro-Raman technique was used extensively to measure stress distribution in LOCOS structures [8, 10, 12 and references given therein]. However interpretation of the Raman results was not easy. Careful experiments of De Wolf[8] showed that as the stripe width decreased, the shape of the Raman frequency versus distance changed qualitatively. Interpretation of these curves acquired urgency[11]. The interpretation of the curves was important both from the academic and technical points of view. In 1995 we showed that FE calculations predict such a change[11]. However the calculated and observed frequencies did not agree quantitatively. It is only recently that we have succeeded in interpreting the spectra quantitatively[13-15].

Pseudomorphic GeSi strained layers on Si substrate and InGaAs layers on GaAs substrates were fabricated and studied in late 1970s and in 1980s (refs 2, 6, 7). Large stresses in the epilayers and substrates are caused due to difference in the lattice constants of the epilayers and the substrates. The lattice mismatch is measured by the misfit parameter f_m defined below[2]:

$$f_m = \frac{a_l - a_{sub}}{a_{sub}}. \quad (1)$$

Here a is the lattice constant and subscripts l and 'sub' indicate the epilayer and the substrate. When a heterostructure is cooled from high temperatures, the difference in lattice constants can also arise due to difference in coefficients of thermal expansion. Stress caused by the lattice or thermal mismatch plays an important and beneficial role in the strained layer devices. Raman technique has been used successfully in measuring stresses in lattice mismatched epilayers[2,4,7]. More recently Raman spectra and stress distribution in the lattice mismatched stripes and quantum wires and in the substrates on which they are grown has been studied[4,11,13,16-18].

In the large area strained epilayers, the stress in the growth plane is uniform and interpretation of Raman experiments is straightforward. However when the strain is highly nonuniform (e.g. in LOCOS structures and quantum wires), it is not easy to interpret the Raman experiments. The diameter of the laser beam and the wavelength of the light used (which determines the absorption coefficient α and the penetration depth) have a large effect on the observed Raman spectra[19]. The calculation of the spectrum, and interpretation of the experimental results becomes very difficult. In this paper we review our recent work on interpretation of the Raman spectra observed from *nonuniformly* strained structures described in our recent papers.

Stresses in the stripes

A schematic diagram of the stripe and substrate structures used in experiments[4,5] is shown in Figure 1. In Figure 1 *a* the virtual substrate and stripe are lattice mismatched. The thickness of the virtual substrate is so large that the main substrate plays no role in determining the stress distribution. We designate such structures as α structures. Unlike in the case of the α structures, in β structures shown in Figure 1 *b* the width of the stripe and the substrate are not equal.

The lattice planes of a compressed pseudomorphic stripe and the substrate on which it is grown are shown in Figure 2 *a*. The structure shown in Figure 2 *a* has not yet been allowed to relax to the lowest energy state. When the system is allowed to relax, the stripe expands at the edges because it is under compression. In so doing it pulls the substrate planes away from the center. The compression in the stripe is reduced and a tensile stress is created in the substrate. The displacements of the lattice planes in the relaxed stripe and the substrate

were calculated using the FEM and are shown in Figure 2 *b*. Before our work[11], it was not recognized that the displacements and stresses in the stripe and the substrate are strongly coupled. Any approximation made to treat one of them separately or loosely coupled to the other gives large errors. It is for this reason that analytical methods are not able to describe the stresses in such structures satisfactorily. Numerical computer calculations are necessary[11].

Extensive measurements of strain induced luminescence- and Raman-shifts have been made in strained GaAs/Si stripes[5] and GeSi/Si stripes[6]. In the stripes the in-plane stresses in the x and y directions are not equal. A further complication arises due to the fact that the stripes are usually grown in a [110] direction and the semiconductors are not isotropic. We found that the secular equations connecting the stress and the luminescence- or Raman-shifts can be solved analytically for the relatively simple case of stripes provided we confine our attention to the middle of the surface layer[20]. This allowed us to develop a method to calculate the splitting and shift of the Raman modes and photoluminescence (PL) peaks due to stresses. The method takes into account the anisotropy of the semiconductor. Using this method the relation between the normalized stress $\alpha' = \sigma_{xx}/\sigma_0$ (in the middle at the surface of the stripe), misfit parameter f_m and shift ΔE in the PL peak is plotted in Figure 3 *a*. We have made similar plots for the relation between α', f_m and the observed Raman shift $\Delta\omega_3$. For any given value of f_m and observed value of the shift in the PL peak or Raman frequency the value of normalized stress α' in the center of the surface layer can be read from these graphs. Using these graphs we have calculated the stresses in the stripes using observed values of luminescence and Raman shifts given in the literature. These values of stresses (shown by symbols) are compared with the FE calculations in Figure 3 *b*. The agreement between the calculated and the experimental values is satisfactory.

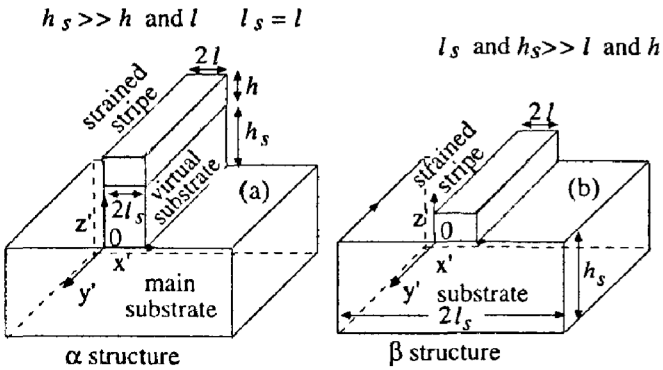

Figure 1. Schematic diagram of the stripe-substrate samples. Origin of x is not always at the edge of the stripe as shown in this figure.

General case of nonuniform stress and Raman scattering

Earlier work

A schematic diagram of a LOCOS structure, axes of coordinates and the laser beam is given in Figure 4. As shown in Figure 2, the structure is highly strained. The penetration depth can vary from a few nanometers to more than several microns or millimeters depending upon the absorption coefficient α of the semiconductor for the laser light used. The diameter of the beam is about ~ 1 μm if the beam is focused and is quite large if the beam is not focused. The beam samples a large volume of the strained structure. In a Raman experiment photons originate from different points (x, z) in the volume of the structure sampled by the laser light. The strain-induced shift of the Raman spectrum from the point (x, z) (measured from unstrained Si shift at 521 cm^{-1},

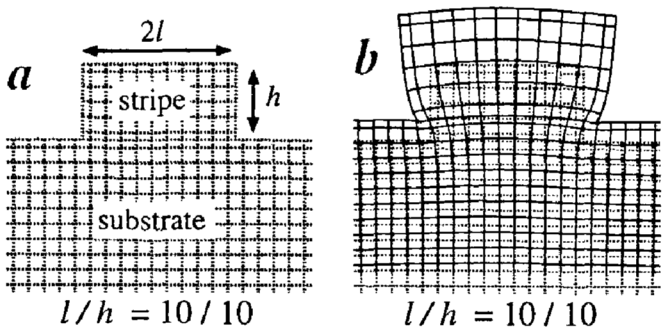

Figure 2. *a*, A compressed stripe grown coherently on a substrate. This situation arises when GeSi/Si or InGaAs/GaAs stripe-substrate structures are fabricated. *b*, The dotted lines show the original structure and the continuous lines show the relaxed structure. The displacements shown by the continuous lines have been multiplied by a factor 15 for clarity[21].

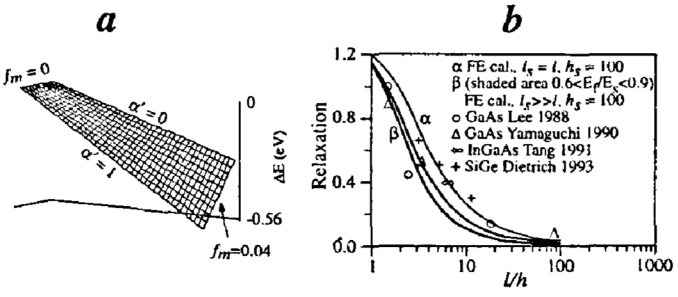

Figure 3. *a*, Surface plot of luminescence-shift ΔE versus misfit parameter f_m and stress for a GaAs stripe. *b*, Comparison of experimental Raman and luminescence data (symbols) and calculated values (curves) of stress relaxation $1 - \sigma_{xx}/\sigma_0$ in stripes. FE values of stresses for $0.6 < E_f/E_s < 0.9$ for β samples are shown by the shaded area. (E_f and E_s are the Young's moduli for the epilayer and the substrate.) References to original papers are given in (ref. 7) from where this figure has been taken.

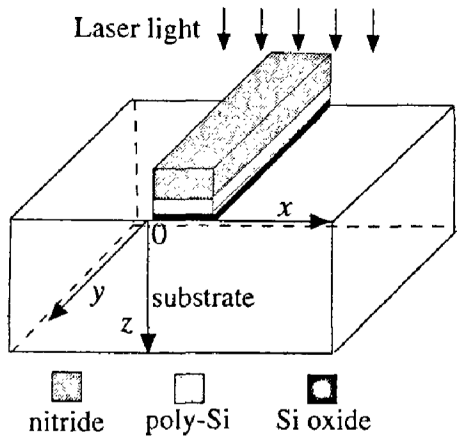

Figure 4. Schematic structure of a LOCOS sample, axes of coordinates and laser beam.

ref. 4) is denoted by $\Delta\omega_3^p(x, z)$ (the superscript p indicates peak frequency of the spectrum). If the stress is not uniform, spectra originating from different points are different from each other. The superposition of these spectra constitutes the final spectrum observed in the experiment. The peak position of this spectrum is the observed Raman shift $\Delta\omega_{3(\text{eff})}$. It is not clear how the shift $\Delta\omega_{3(\text{eff})}(x_0)$, ($x_0$ is the position of the unfocused laser beam) is related to the shifts, $\Delta\omega_3^p(x, z)$, of the individual spectra or to the stress distribution $\sigma(x, z)$. If the beam is focused at $z = z_0$, the spectra depend on z_0 also.

The problem was first addressed by Harker and Jain[12] and later by Jain *et al.*[19] and De Wolf *et al.*[9]. The method used in these early papers was not correct. In the method used in[9,12,19] the peak position $\Delta\omega_3^p(x, z)$ of each individual spectrum was assumed to be proportional to the intensity of light and independent of the depth at which the light was focused. The following equations were used to calculate the average position $\Delta\omega_3^a(x_0)$ of the Raman peak:

$$\Delta\omega_3^a(x) = \frac{\int_0^{z_1} \Delta\omega_3^p(x, z) I_f(z)\, dz}{\int_0^{z_1} I_f(z)\, dz}, \tag{2}$$

$$\Delta\omega_3^a(x_0) = \frac{\int_{x_1}^{x_2} \Delta\omega_3^a(x) I_f(x, x_0)\, dx}{\int_{x_1}^{x_2} I_f(x, x_0)\, dx}, \tag{3}$$

$$I_f(x, x_0, z) = I_0 I_f(x, x_0) I_f(z), \tag{4}$$

$$I_f(z) = \exp(-2\alpha z), \tag{5}$$

and

$$I_f(x, x_0) = \exp\left(-2\frac{(x - x_0)^2}{B^2}\right). \tag{6}$$

$\Delta\omega_3^a(x)$ is the average of $\Delta\omega_3^p(x, z)$ over depth z, weighted with the intensity of light $I_f(z)$. Similarly $\Delta\omega_3^a(x_0)$ is the average of $\Delta\omega_3^a(x)$ over x weighted with $I_f(x, x_0)$. $I_f(x, x_0, z)$ is the intensity of the scattered light from the point (x, z) (see Figure 4) and emerging at the surface of the structure. The light beam is assumed to be parallel. The light intensity is taken to vary independently in the x and z directions and is given by eq. (4) where I_0 is the intensity at the center of the incident beam. I_0 can be taken to be unity without loss of generality. The variation of light intensity with x and z is given by eqs (5) and (6). The factor 2 in eq. (5) arises because the light traverses the distance to the point z twice. $2B$ is the beam width at $I_f(x, x_0)/I_0 = 1/e^2$. B is taken to be 1 μm in the calculations. The upper limit of integration in eq. (2) is usually taken to be equal to $1/\alpha$. Numerical results using these equations have been published by Jain *et al.*[19] for semiconductor stripes grown on substrates and more recently by De Wolf *et al.*[9] for LOCOS structures.

Eqs (2) and (3) are based on intuition and have no physical justification. In particular the Raman shift $\Delta\omega_3^p(x, z)$ is not affected by the light intensity $I_f(x, x_0, z)$ and taking its average weighted with $I_f(x, x_0, z)$ is not correct. The errors involved in the results obtained using these equation cannot be estimated.

The correct method to synthesize the 'observed Raman spectrum', the case of parallel beam

First we consider a parallel incident light beam and assume that the spectrum originating from the point (x, z) is given by a Lorentzian with halfwidth $A = 1.4$ cm^{-1} (ref. 14). The halfwidth includes the natural line width and the detector resolution. The Raman intensity $I(\Delta\omega_3, x, x_0, z)$ can be written as[13],

$$I(\Delta\omega_3, x, x_0, z) = \frac{I_f(z) I_f(x, x_0)}{\left(\frac{\Delta\omega_3 - \Delta\omega_3^p(x, z)}{A}\right)^2 + 1}. \tag{7}$$

This equation assumes that all scattered photons are equally likely to be detected. The peak frequency $\Delta\omega_3^p(x, z)$ depends on all the strain components at the point (x, z) and is obtained by solving numerically the secular equation which describes the relation between the Raman shift and the strain[4,9,20]. Spectra from all

(x, z) points (see Figure 4) are superposed to obtain the intensity $I(\Delta\omega_3, x_0)$ of the final spectrum,

$$I(\Delta\omega_3, x_0) = \int_{-\infty}^{\infty} I(\Delta\omega_3, x) I_l(x, x_0)\, dx, \tag{8}$$

where

$$I(\Delta\omega_3, x) = \frac{I_l(z)\, dz}{\int_0^{\infty} \left(\frac{\Delta\omega_3 - \Delta\omega_3^p(x, z)}{A}\right)^2 + 1}. \tag{9}$$

For a thick sample the upper limit of integration (performed numerically) in eq. (9) should be chosen at z_1, where z_1 is sufficiently large such that the integration to larger depths does not change the result appreciably. We will see later that if we use $z_1 \sim 1/\alpha$, we do not obtain accurate results. It is necessary to use values of z_1 which are larger than $1/\alpha$.

In the new method it is the intensity of Raman light, and not the Raman frequency which is modulated by the intensity of the incident light. Unlike the previous method, no averages are taken, the spectra originating at different points in the sample are superposed.

The case of focused beam

The results obtained with a focused beam are quite different from those obtained with the parallel beam. To interpret Raman spectra obtained with focused beams, we approximate the intensity of light at z by the following equation[13,14],

$$I_{L\,(\text{focus})}(z, z_0) = \frac{p^2 I_l(z)}{(z - z_0)^2 + p^2}. \tag{10}$$

Here z_0 is the depth at which the beam is focused and p is an adjustable parameter. The variation of $I_{L\,(\text{focus})}(z)/I_{L\,(\text{focus})}(0)$ with z for $\alpha = 35.63 \times 10^5\ \text{m}^{-1}$ (ref. 9) is shown in Figure 5, for several values of p and for $z_0 = 0$ in Figure 5 *a*. Similar results for $z_0 = 530$ nm are shown in Figure 5 *b*. It is seen that the normalized intensity is a strong function of p until p becomes larger than about 1000 nm. In Figure 5 *a* it decreases with p whereas opposite is the case in Figure 5 *b*. For $p \geq 3000$ nm, plots of $\exp(-2\alpha z)$ agree with curve 1 to better than 2%. The error becomes smaller as p increases and is reduced to less than 1% for $p = 4000$ nm. Furthermore, the fact that curves 2 and 3 in Figure 5 *a* and curve 2 in Figure 5 *b* can be fitted with $\exp(-2\gamma\alpha z)$ shows that in these cases the effect of focusing the beam is only to change the effective absorption coefficient of the laser light. For integration of eq. (9) the focused beam can be taken as a parallel beam with a new absorption coefficient given by $\gamma\alpha$ provided that $p \gtrsim 1/\alpha$. In Figure 5 *a* the light behaves as if it is more strongly absorbed and penetrates shorter distances in the substrate. This can be used to explore the region near the surface. In Figure 5 *b* the effective absorption coefficient is weaker and light penetrates larger distances in the substrate.

Unfortunately there is no simple way of determining p in any given case. Among other things, it depends on the optical arrangement of the instrument used in the Raman measurements. Another difficulty with analysing a focused beam is that the diameter B of the beam now depends on z. In principle, the intensity $I_l(x, x_0, z, z_0)$ cannot be separated into two factors, one a function of x only and the other of z only. We have neglected the interdependence of x and z variations here. We will see later that our model describes experimental results well.

Effect of depth of integration

In this section we discuss our unpublished work[21] on the effect of magnitude of z_1 on the calculated Raman spectra. Consider the sample shown in Figure 6. All components of stress and strain in the sample were calculated using the FE method[4,5,20]. As an example the component $\varepsilon_{s,xx}$ in the substrate calculated along the dotted line (at $x = x_0 = 3.2\ \mu\text{m}$) is shown by curve 1 in Figure 6. The secular equation which gives the relation between the strain components and the Raman shift[4,5,9,20] was solved numerically to calculate the Raman shifts $\Delta\omega_3^p(x_0, z)$. The values of Young's moduli used in the calculations are 150 GPa for the stripe and 130 GPa for the substrate. The phonon deformation potential values are $K_{11} = -1.85$, $K_{12} = -2.3$, and $K_{44} = -0.7$ for the Si

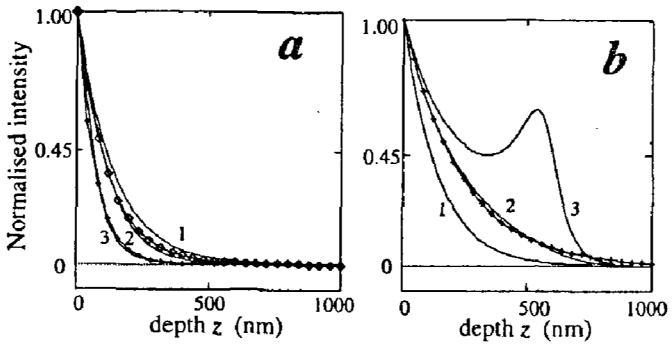

Figure 5. Plots of normalized light intensity $I_{L\,(\text{focus})}(z)/I_{L\,(\text{focus})}(0)$ versus z (see eq. 10). *a*, Beam focused at the surface. *b*, Beam focused at 530 nm below the surface. Curves labelled 1 are identical in both figures and are for $p = 3000$ nm. These curves become practically independent of p for $p \geq 3000$ nm. Curves 2 are for $p = 300$ nm, and curves 3 are for $p = 100$ nm. The symbols are the empirical fits of $\exp(-2\gamma\alpha z)$, plus-sign symbols are for $\gamma = 2$ in (*a*) and 0.6 in (*b*) and diamonds are for $\gamma = 1.2$.

substrate. All components of strain were included in this calculation. The values of $\Delta\omega_3^p(x_0, z)$ (at $x = x_0 = 3.2$ μm) obtained as a function of z in this manner are shown by curve 2 in Figure 6. The effect of depth on the synthesized Raman spectra for this case is discussed later in this section.

To study in detail the effect of depth of integration, we also analysed a problem which could be solved analytically[21]. The analytical solution is expected to give more insight into the physics involved. We assume a distribution of strain such that the Raman frequency $\Delta\omega_3^p(z)$ is given by

$$\Delta\omega_3^p(z) = \Delta\omega_3^p(0)\exp(-\beta z). \quad (11)$$

We assume that the stress does not vary in the x and the y directions. Eq. (9) with $\Delta\omega_3^p(x, z)$ given by eq. (11) can be integrated analytically for $\alpha/\beta = 0, 0.25, 0.5$ and 1. The Raman spectra for $\alpha = 0$ and $\beta = 35.63 \times 10^5$ m^{-1} are shown in Figure 7. The results of the calculations made for several values of depth z_1 are shown in Table 1 for $\alpha = 0$ and Table 2 for $\alpha = \beta$. The shifts in column 2 of Table 1 are positive because eq. (11) implies a compressive strain. Figure 7 and Table 1 show that for a transparent material with $\alpha = 0$, $\Delta\omega_{3(\text{eff})}^p$ keeps changing with z_1 up to very large values of z_1.

In column 2, the value of $\Delta\omega_{3(\text{eff})}^p$ has become very small (0.03 cm^{-1}) at $z_1 = 10$ μm but additional calculations showed that it has not yet reached a constant value. It keeps decreasing with z_1 and approaches zero asymptotically as $z_1 \to \infty$. Since the resolution in the experiments is not better than 0.03 cm^{-1}, the observed spectrum for $z_1 > 10$ μm corresponds to that of unstrained Si with zero shift.

Raman studies with unattenuated light are often made to measure strains in semiconductor heterostructures[22]. The present calculations show that unattenuated light in a parallel beam is not suitable for such measurements with thick substrates if the substrate material has a Raman line close to the line being used for measuring the strains. Raman measurements with unattenuated light are incapable of giving any information about the strain distribution in the upper part of a thick (> 10 μm) Si substrate.

It is also seen from Figure 7 that the intensity of the spectrum increases with z_1. In curve 4, the peak intensity is almost 100 times larger than that of curve 1. This increase is partly related to an increase in the total number of scatterers and to the variation of stress with z. Near the interface $\Delta\omega_3$ varies rapidly with z and the number of atoms that scatter in the interval $\Delta\omega_3$ and $\Delta\omega_3 + d\Delta\omega_3$ at any given frequency $\Delta\omega_3$ is small. As z increases, variation of $\Delta\omega_3$ becomes slow. Therefore the number of scatterers in the interval $d\Delta\omega_3$ increases with z_1. In this case also $\Delta\omega_{3(\text{eff})}^p \to 0$ as $z_1 \to \infty$.

Results of numerical calculations made for the sample described in Figure 6 are given in column 3 of Table 1 (ref. 23). The shift, $\Delta\omega_{3(\text{eff})}^p$, has not become as small as in the first case at $z_1 = 10$ μm. This is due to the fact that for large values of z the strain decays more slowly and penetrates to larger depths in this case. For example, curve 2 in Figure 6 shows that at 1 μm $\Delta\omega_3^p(x_0, z)$ is reduced to 12% of its maximum value but in the previous case (eq. 11) it is reduced to 3% of its maximum.

Results of calculations similar to those given in Table 1 but for $\alpha > 0$ are given in Table 2. For 457.9 nm laser light used in many experiments[9], the value of α is 35.63×10^5 m^{-1}. Table 2 shows that the calculated shift

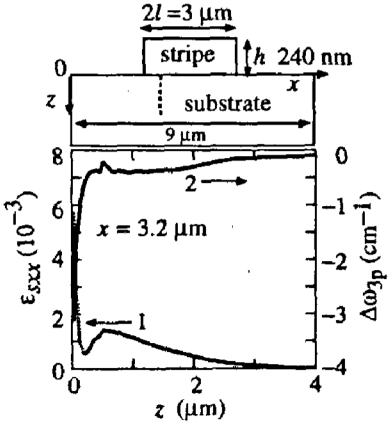

Figure 6. The stripe shown at the top is compressed with a lattice mismatch of 2%, which corresponds to a stress $\sigma_0 = 4$ GPa. Curve 1 shows the (tensile) strain component $\varepsilon_{xx}(x, z)$ in the substrate at $x = 3.2$ μm (calculated by the FE method along the vertical dotted line), curve 2 is the corresponding Raman shift $\Delta\omega_3^p(z)$ calculated numerically[21].

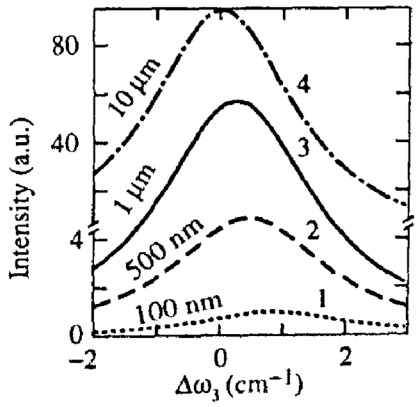

Figure 7. Calculated spectra for a parallel beam probe using the analytical model (see eq. (11)). The values of $\alpha = 0$ and $\beta = 35.63 \times 10^5$ m^{-1} were used in the calculations. The depths z_1 up to which the integration was performed are given on the curves[24].

does not become constant until z_t exceeds 600 nm, a length considerably larger than the value of $1/\alpha$. The value of β in eq. (11) is 4α which gives a characteristic length $= 1/\beta = 70$ nm for the strain distribution. 600 nm is also $> 1/\beta$. At $z = 600$ nm the light intensity has decreased to $\sim 2\%$ of its maximum value at $z = 0$. Calculations made for several other cases show that in most cases the final shift becomes constant (i.e. independent of z_t) only when z_t is so large that the light intensity has fallen to about 2% of its maximum value. If strain becomes small earlier, the contribution of the unstrained Si becomes large and the observed shift corresponds more nearly to that of unstrained Si even for $\alpha > 0$. For the FE case given in column 3 of Table 2, $\Delta\omega^{p}_{3(\text{eff})} = -1.18\ \text{cm}^{-1}$ corresponds to a strain of $1.13 \times 10-3$ as opposed to the strain near the interface, which is more than 5 times larger. We therefore conclude that lasers with relatively short wavelength light (with $1/\alpha = 5$ to 10 nm) are better for measuring strain near the interface in Si heterostructures using Raman experiments. This light will decay to 2% of its maximum value at a depth of 10 to 20 nm. The observed shift will correspond to some average of stress in this depth. Actual shift will depend on the details of distribution of stress. As discussed earlier surface region can be explored with long-wavelength light by focusing the beam at or above the interface. The calculations made in this section are for parallel beam but in most cases the conclusions are valid for the case of the focused beam also.

The intensity of the contribution to the spectrum originating at z is $\exp(-2\alpha z)$ and it falls to $1/e^2$ at $z = 1/\alpha$. It seems reasonable to assume[9] that the contribution from larger depths would be negligible. The results discussed above show that this is not the case. Large contribution to the observed spectrum can come from much larger depths using a parallel probe beam. If the beam is focused below the interface, effective wavelength of light decreases and the light penetrates even larger distances (see subsection 'The case of focused beam').

Table 1. Calculated peak positions $\Delta\omega^{p}_{3(\text{eff})}$ for $\alpha = 0$ and for several values of depths z_t over which the integration was performed. The results given in column 2 are based on the strain distributions given by eq. (11). FE calculations were made for the sample shown in Figure 6 at $x_0 = 3.2\ \mu$m and are shown in column 3

Depth z_t	$\Delta\omega^{p}_{3(\text{eff})}(x_0)$ (cm^{-1}) $\beta = 35.63 \times 10^5$ m^{-1} in eq. (11)	$\Delta\omega^{p}_{3(\text{eff})}(x_0)$ (cm^{-1}) FE for Figure 6
100 nm	0.84	−1.86
300 nm	0.61	−0.81
500 nm	0.46	−0.56
1 μm	0.26	−0.44
10 μm	0.03	−0.10

Effective depth and shape of Raman lines

We now discuss the effective depth[15]. The effective depth is defined in such a manner that the strain at this depth corresponds to the observed Raman peak frequency. We consider a sample shown in Figure 8 *a*. The strain distribution along the dotted line in the substrate is given in Figure 8 *b*. The intensity of the Raman shifts $\Delta\omega^{p}_{3}(z)$ and calculated Raman spectrum are plotted in Figure 8 *c*, and the relation between the $\Delta\omega^{p}_{3}(z)$ and z is shown in Figure 8 *d*. The zero of the shifts is at the Raman frequency 521 cm^{-1}. If the laser light is not attenuated by absorption, the intensity of the peaks $\Delta\omega^{p}_{3}(z)$ plotted along the y-axis in Figure 8 *c* will be of equal height. As we go deeper the intensity of the Raman spectrum diminishes because of the absorption of light ($\alpha = 35.63 \times 10^5$ m^{-1}) and numerical

Table 2. Same as Table 1 but for $\alpha = 35.63 \times 10^5$ m^{-1}

Depth z_t (nm)	$\Delta\omega^{p}_{3(\text{eff})}(x_0)$ (cm^{-1}) $\beta = 4\alpha$ in eq. (11)	$\Delta\omega^{p}_{3(\text{eff})}(x_0)$ (cm^{-1}) FE for Figure 6
100	0.57	−2.10
300	0.37	−1.41
500	0.33	−1.22
700	0.32	−1.18
800	0.32	−1.18

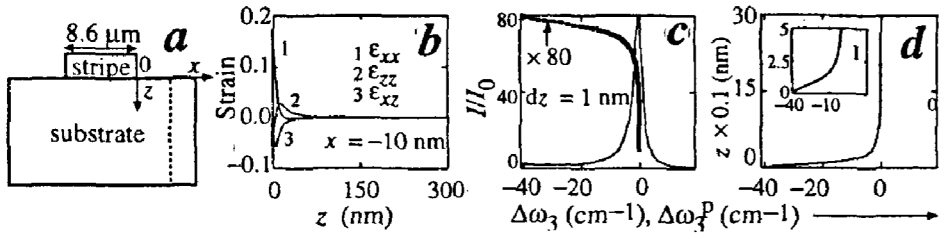

Figure 8. *a*, Sample structure: a compressed stripe (with a lattice mismatch of 2%) on a Si substrate. *b*, Strain components calculated along the dotted vertical line in (*a*). *c*, Intensity of the Raman peaks multiplied by the intensity of light (crosses which appear like a thick line) and the final Raman spectrum (thin curve). Zero on the x-axis corresponds to Si frequency at 521 cm^{-1}. *d*, Strain-induced Raman shifts at different depths z.

value of the shift becomes smaller because the strain decreases. The calculated Raman spectrum is also shown in Figure 8 *c*. The shift of the peak frequency is small, it is only $-0.35\,cm^{-1}$. This shift corresponds to a strain which exists at a depth of $z = 100$ nm. Therefore the effective depth in this case is 100 nm. This demonstrates again that the Raman spectrum gives practically no information about the strain distribution near the interface. Long wavelength laser light with small values of α tend to give the Raman shift corresponding to the deeper regions where strain and its variation are small.

We also calculated the Raman spectra for 4 different values of the absorption coefficient α (ref. 15) (see Figure 9). The figure shows that for large α and small penetration depth, the Raman line is highly asymmetrical. The crosses (which appear like thick lines in the figure) are the plots of the Raman shifts which are a measure of the strain. In the lower figures, for large values of α, the right hand portion of the spectrum practically coincides with the shifts. Therefore the right hand portion of the spectrum can be used as a rough measure of the strain distribution. As α decreases and the penetration depth increases, the right hand side of the spectrum does not agree with the distribution of the Raman shifts. A second peak begins to appear in the spectrum. For larger penetration depths the spectrum becomes identical with that shown in Figure 8 *c*. The discussion as to why lower regions dominate given earlier and in our papers[14,15] provides a physical interpretation of the effect of α on the line shape.

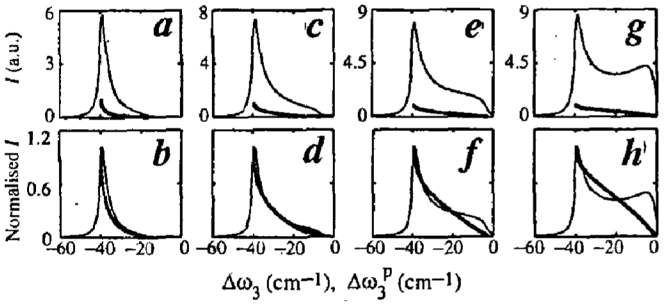

Figure 9. Thin curves: Plots of the calculated spectra from non-uniformly strained structure of Figure 8 *a* for 4 different values of α. The strain components are the same as given in Figure 8 *b*. Thick lines consisting of crosses: The intensity $\exp(-2\alpha z)$ of the strain-induced Raman shifts $\Delta\omega_3^0(z)$ plotted as a function of the shifts. The curves in the figures at the bottom have been normalized with their own maxima. The values of α are: *a* and *b* for $\alpha = 1.98 \times 10^8\,m^{-1}$ and $2/\alpha = 10$ nm; *c* and *d* for $\alpha = 1.05 \times 10^8\,m^{-1}$ or $2/\alpha = 19$ nm; *e* and *f* for $\alpha = 0.69 \times 10^8\,m^{-1}$ or $2/\alpha = 29$ nm; and *g* and *h* for $\alpha = 0.44 \times 10^8\,m^{-1}$ or $2/\alpha = 46$ nm.

Comparison with experiment

Local oxidation of silicon

We have used the procedure discussed above in the subsection 'The case of focused beam' to interpret micro-Raman experiments on the local oxidation of silicon (LOCOS) samples. The structure of the LOCOS samples is shown in Figure 10 *a*. Experimental Raman shifts from these samples have been reported in ref. 4.

In these experiments light was focused at $z_0 = 530$ nm below the poly-Si/Si interface. The Raman spectra were synthesized using the method described in the subsection 'The case of focused beam'. The parameter p was used as a fitting parameter. Best results were obtained for $p = 600$ nm. The contribution to the Raman spectra from the poly-Si buffer was included in the calculated spectra. The calculated values of $\Delta\omega^P_{3(\text{eff})}(x_0)$ are compared with the experimental results in Figure 10 *b* for the 3 μm sample and in Figure 10 *c* for the 5 μm sample. The agreement between the theory and the experiment is very good in both cases. Earlier attempts to calculate the Raman spectra were not so successful[4]. The salient points of our work which made it possible to obtain such good agreement between the model calculations and the experiment are: The effects of laser beam width and penetration depth were taken into account correctly, the focused beam was used (i.e. it was not approximated

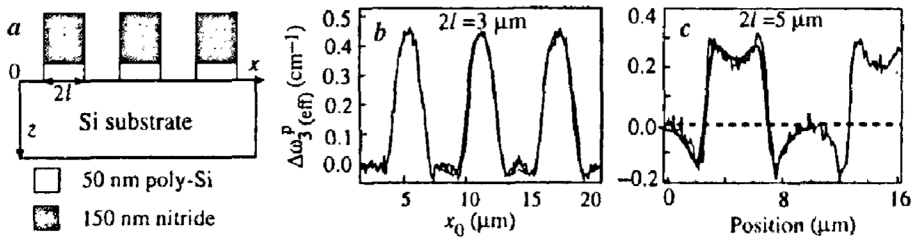

Figure 10. *a*, Schematic structure of the LOCOS samples. *b* and *c*, Comparison of experimental results (thin curves) with those calculated by the present method (thick curves). The calculated curves are not shown for the first peak in the 3 μm sample in (*b*) and for the second peak in the 5 μm sample in (*c*) to show clearly the experimental results and to demonstrate the excellent agreement between the calculated and the observed Raman shifts.

by a parallel beam), the stresses in the polysilicon layer were taken into account, and the effect of light scattered from depths $> 1/\alpha$ on the Raman shift was included.

Quantum wires

Stresses in quantum wires and quantum dots are important for determining their optical and transport properties and for fabricating devices with enhanced performance[2,4,5,16]. Dietrich *et al.*[16] have reported Raman spectra of $Ge_{0.11}Si_{0.89}$ quantum wires of 4 different widths $2l$. The structure of the wires is shown in Figure 11. Raman measurements were made in the back-scattering geometry using the $\lambda = 514.5$ nm line of an Ar^+-ion laser. The laser beam was centred in the middle of a quantum wire.

We calculated the stresses in the quantum wires by the FE method[4,11]. The values of elastic constants and other parameters used in the calculations are given in Table 3. 11% Ge in the $Ge_{0.11}Si_{0.89}$ layer corresponds to a lattice mismatch of 0.0046 with Si substrate[13]. The calculated stress in the substrate was practically zero (see Figure 12). Therefore the neighbouring wires do not interact with each other. The calculated stresses in a wire are shown in Figure 12. There is a large tensile stress in regions 11 in the Si layers and a large compressive stress in region 2 in the GeSi layer (Figure 12 *a*). In these regions the stress reaches values up to $\sim \pm 500$ MPa. All the stress components are shown as a function of z at two values of x in Figure 12 *b*. The component σ_{xx} dominates near the interfaces. Dietrich *et al.*[16] calculated the Raman shift considering the stress in the GeSi layer only. Figure 12 *b* shows that considerable tensile stress exists in Si layers. The contribution of stressed Si to the Raman line is quite large.

The integration in eq. (8) was performed for x varying from -1.35 μm to 1.35 μm, encompassing 9 wires, and in eq. (9) for z varying from 0 to 2 μm. While integrating over depth Si parameters were used in Si region and the GeSi parameters were used in GeSi region. The scattering factor (the strength of scattered Raman light) for the GeSi layer is 2.9 times larger than that of Si (ref. 14). Values of all constants used in the calculations are given in Table 3. The calculated spectrum from the 9 wires including the contribution of unstrained Si substrate is shown in Figure 13. The best fit was obtained by using $p = 4$ μm. The curves in this figure have been normalized so that the Si peak height is the same as that of the observed spectrum. We superposed all the spectra originating at different z for two fixed values of x, $x = 60$ nm and at $x = 0$ nm. These spectra are shown by curves 1 and 2 in Figure 13 *a*. This figure shows the strong dependence of the spectrum on x_0, the position of the laser beam. It also shows that the Raman shift does not give a direct measure of the stress or strain at any given depth. The final spectrum obtained by superposition of the spectra from all the points in the volume sampled by the laser light is shown in Figure 13 *b*. The observed spectrum is shown in Figure 13 *c*.

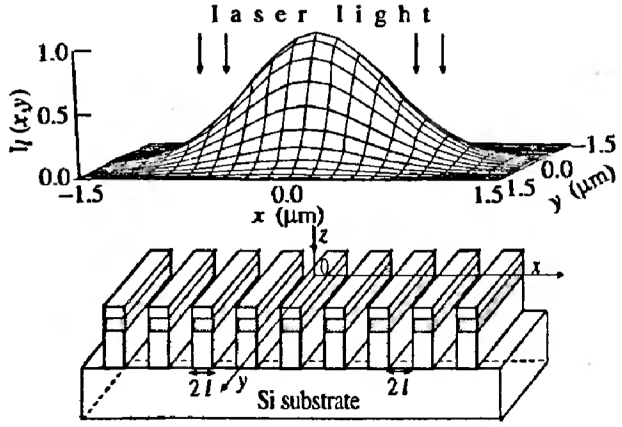

30 nm Si cap, 50 nm $Ge_{0.11}Si_{0.89}$ and 100 nm Si quantum wires. $2l = 150$ nm. □Si, ▨50 nm $Ge_{0.11}Si_{0.89}$

Figure 11. Structure of the quantum wires, the laser beam and the axes of coordinates.

Table 3. Constants used in the calculations. FWHM is full width at half maximum of the Raman spectrum. K_{11}, K_{12}, and K_{44} are the phonon deformation potentials

Constants	Si	$Ge_{0.11}Si_{0.89}$	Refs
K_{11}	−1.85	−1.806	4
K_{12}	−2.3	−2.256	4
K_{44}	−0.7	−0.744	4
Young's modulus (GPa)	130	127	25
Poisson's ratio	0.28	0.277	25
2A (FWHM) (cm^{-1})	3.5	6.8	16
α (10^5 m^{-1})	9.5	38	26

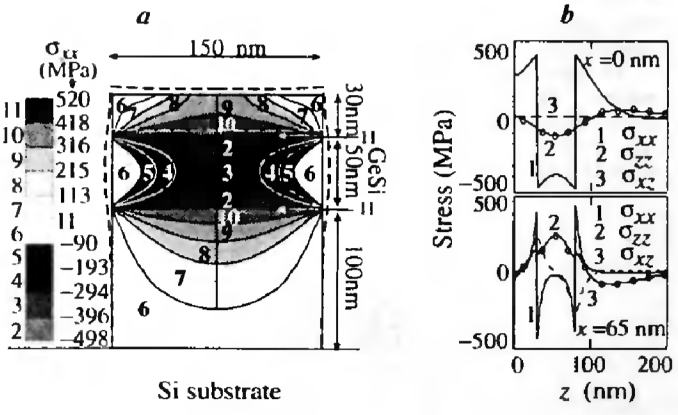

Figure 12. *a*, shows the stress components σ_{xx} in the quantum wire (shown in Figure 11) calculated by the FE method. Solid vertical and horizontal lines show the outer contour and interfaces before relaxation. The displaced surfaces and interfaces after the relaxation are shown by the dashed lines. The displacements are shown multiplied by a factor 14 for clarity. The dashed line for the lower interface between the GeSi and Si layers is hidden behind the narrow region 11 of high stress and cannot be seen. *b*, shows all the stress components as a function of z at two positions, near the edge at $x = 65$ nm and at the center at $x = 0$ nm.

The calculated spectrum is compared with the observed spectrum in Figure 13 *d*. The agreement between the two spectra is excellent. The curve in Figure 13 *b* is different from both the curves in Figure 13 *a*. This emphasizes the importance of the effect of *width* of the laser beam. Our calculations can be used to determine separately the contributions to the spectrum from different parts of the structure. We find that curve 3 is a composite peak, a part of it originates from the compressively stressed GeSi layer and the other part from Si layers which are under tensile stress. The contributions to this peak from stressed GeSi and Si are comparable.

Other structures

Raman spectra of ZnSe epitaxial layers grown on GaAs substrate using lasers of two different wavelengths, 413.1 nm and 488 nm light have been reported[26] for different thicknesses of ZnSe layers. ZnSe is transparent for 488 nm and 413.1 nm light penetrates a distance of ~ 50 nm (ref. 26). The spectra from the 180 nm thick layer are shown in Figure 14. The lattice mismatch between ZnSe and GaAs is 0.27%, the lattice constant of ZnSe is bigger. The LO Raman frequency for unstrained bulk ZnSe is shown by the arrow in the figure, it is 256.3 cm^{-1}. The strain-induced shift in the Raman line measured with the 488 nm light is ~ 1.14 cm^{-1} whereas the shift measured with the 413.1 nm laser light is ~ 0.7 cm^{-1}. The corresponding values of strain are 0.0027 and 0.0023 respectively. To interpret these results Olego *et al.*[24] suggested that the strain in the top part of the layer is smaller than in the lower part. The shift measured with 413.1 nm light was attributed to the strain in the top 50 nm of the layer and the shift measured with the 488 nm light was assumed to give the average over the whole thickness. We have shown in ref. 21 that this explanation is not correct. We assumed several plausible values of strain distribution with depth and computed the observed spectrum using the method outlined in the subsection 'The correct method to synthesize the "observed Raman spectrum", the case of parallel beam'. The calculated spectrum could be made to agree with the observed spectrum only if the strain at the interface is assumed to be more than the lattice misfit of 0.27%, an impossible situation. Since the strain near the interface cannot be larger than the lattice mismatch, these results rule out the possibility that the difference between the 488 and 413.1 nm spectra is due to the increase of strain in the lower part of the layer. We also showed that for the likely dimensions used in the experiment, the edge-induced relaxation would be negligible. We looked for other possible explanation to interpret these experiments.

In most cases interfaces between two semiconductors give rise to new Raman modes (ref. 22 and references given therein) designated as interface modes or IFMs. In some heterostructures, neither cations nor anions are common on the two sides of the interface. ZnTe/CdSe and InAs/GaSb are examples of such heterostructures. In such cases a particular type of IFM, known as mechanical vibrational interface phonon (MVIF) mode exists. ZnSe like mode has been observed in ZnTe/CdSe superlattices. Similarly InSb and GaAs like modes have been observed in InAs/GaSb superlattices. Raman studies of Ge/Si superlattices show that two monolayer thick disordered GeSi alloy layer is formed at the interface and gives a corresponding IFM peak in Raman spectra. In our paper[22] we have provided evidence that Ga_2Se_3 layer is formed at the ZnSe/GaAs interface. The 258 cm^{-1} Ga_2Se_3 Raman line could overlap with the ZnSe line at 257 cm^{-1} (observed with the 413.1 nm light) and shift this line to higher frequency obtained with the 488 nm light. Since the intensity of 413.1 nm light decreases to < 2% at the interface, the IFM line is not contained in

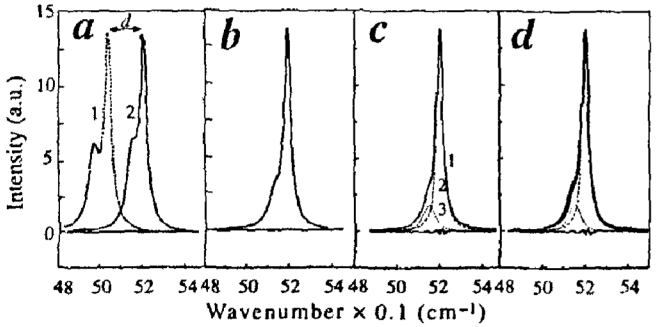

Figure 13. Curve 1 in (*a*) is obtained by applying the laser correction (eq. (9)) in depth only at $x = 60$ nm and curve 2 is the same at $x = 0$ nm. For clarity curve 1 is displaced to the left by the distance *d* as shown. *b*, The final calculated spectrum with full laser correction for beam width and penetration depth. Curve 1 in (*c*), is the observed spectrum and its resolved components into an unstrained Si line (curve 2) and a line due to strain in GeSi and Si layers (curve 3)[16]. The curves in (*b*) and (*c*) are superposed in *d*.

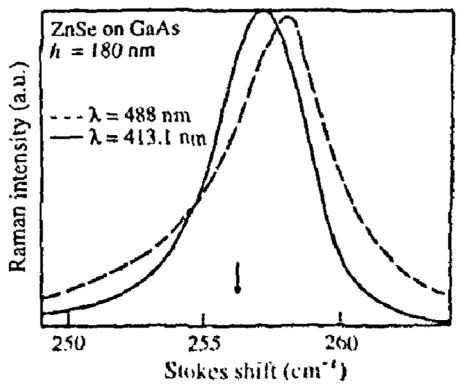

Figure 14. Raman shifts from 180 nm ZnSe epilayer grown on (100) GaAs with 488 and 413.1 nm laser light[24]. The arrow shows the peak position 256.3 cm^{-1} for the unstrained ZnSe.

the spectrum of this light[21]. Studies of ZnSe/GaAs interfaces have shown that highly defective layers are also formed at the interface. We therefore suggested that the Raman line observed with the long wavelength light contains a contribution from IFMs. Unfortunately Raman studies of these interfacial layers have not been made.

We have also applied the correction due to laser beam width and penetration depth to the Raman spectra observed with GaN epilayers[18]. A simple model was developed which could interpret the results satisfactorily.

Concluding remarks

In uniformly strained semiconductors, the value of strain can be determined by measuring the strain-induced shift of the Raman spectrum[4,5]. The situation in non-uniformly strained semiconductors is different. In these semiconductors Raman spectrum strongly depends on the diameter and penetration depth of the laser beam and the spectrum obtained with the focused beam is different from that obtained with a parallel beam. Observed Raman spectrum is related to the nonuniform stress distribution in a very complex way.

Stripe-substrate structures are used in many experiments and in device structures. In most strained stripe-substrate structures, the stress near the interface in the substrate is of practical interest. The stress is maximum near the interface. It decays with depth, rapidly near the interface and slowly at larger depths. If the absorption coefficient α is small and light penetration depth is large, the observed Raman frequency corresponds to deeper regions where the stress and its decay rate are small. The Raman frequency is dominated by these weakly strained lower regions of the substrate. The Raman spectrum gives practically no information about the stress distribution near the interface, a surprising result. A small value of α is not suitable for measuring stresses near the surface or the interface of a heterostructure. Even for large α, the regions for $z > 1/\alpha$ always contribute significantly to the observed Raman shift.

We have obtained extremely good agreement between the calculated and measured Raman spectra in LOCOS structures, quantum wires and other semiconductor devices. To obtain this agreement, it was necessary to take into account the effects of laser beam width and penetration depth, include contributions originating from depths much larger than $1/\alpha$, and not to approximate the focused beam by a parallel beam. The calculations were made on a fast table top PC. Calculations of one spectrum involve calculation of stress tensor by the FE method, solution of the secular equation, calculation of Raman spectra from closely spaced points and synthesizing the final spectrum, all done numerically. Calculation of one spectrum can take up to 30 h of computer time. The method we have developed is general and can be used in structures of any complexity, e.g. IC chips containing variety of overlayers, active components, passive components, trench isolation and interconnects.

1. Raman, C. V. and Krishnan, K. S., *Nature*, 1928, **121**, 501–502.
2. Jain, S. C., *Germanium—Silicon Strained Layers and Heterostructures*, Advances in Electronics and Electron Physics Series, Supplement 24, Academic Press, Boston, 1994.
3. Hu, S. M., *J. Appl. Phys.*, 1991, **70**, R53.
4. Jain, S. C., Maes, H., Pinardi, K. and De Wolf, I., *J. Appl. Phys.*, 1996, **79**, 8145–8165.
5. Jain, S. C., Willander, M. and Maes, H., *Semicond. Sci. Technol.*, 1996, **11**, 641–671; Erratum, *Semicond. Sci. Technol.*, 1996, **11**, 975.
6. Jain, S. C., Maes, H. E. and Van Overstraeten, R., *Curr. Op. Solid-State Mat. Sci.*, 1997, **2**, 722–727.
7. Jain, S. C., Willander, M., Pinardi, K. and Maes, H., *Phys. Scri.*, 1997, **T69**, 65–72.
8. De Wolf, I., Vanhellemont, J., Romano-Rodriguez, A., Norström, H. and Maes, H. E., *J. Appl. Phys.*, 1992, **71**, 898–906.
9. De Wolf, I., Maes, H. E. and Jones, S. K., *J. Appl. Phys.*, 1996, **79**, 7148.
10. De Wolf, I., Pozzat, G., Pinardi, K., Howard, D. J., Ignat, M., Jain, S. C. and Maes, H. E., *Microelectronic. Reliab.*, 1996, **36**, 1751–1754.
11. Jain, S. C., Harker, A. H., Atkinson, A. and Pinardi, K., *J. Appl. Phys.*, 1995, **78**, 1630–1637.
12. Harker, A. H. and Jain, S. C., unpublished work.
13. Jain, S. C., Pinardi, K., Willander, M., Atkinson, A., Maes, H. E. and Van Overstraeten, R., *Semicond. Sci. Technol.*, 1997, **12**, 1507–1509.
14. Pinardi, K., Jain, S. C., Willander, M., Atkinson, A., Maes, H. E. and Van Overstraeten, R., *J. Appl. Phys.*, 1998, **84**, 2507–2512.
15. Pinardi, K., Jain, S. C., Maes, H. E., Van Overstraeten, R., Willander, M. and Atkinson, A., *MRS Symp.*, 1998, **505**, 507–512.
16. Dietrich, B., Bugiel, E., Frankenfeldt, H., Harker, A. H., Jagdhold, U., Tillack, B. and Wolff, A., *Solid-State Electronics*, 1996, **40**, 307.
17. Jain, S. C. and Maes, H. E., *Thin Solid Films*, 1997, **292**, 218–226.
18. Jain, S. C., Pinardi, K., Maes, H. E., Van Overstraeten, R., Willander, M. and Atkinson, A., *MRS Symp.*, 1998, **482**, 875–880.
19. Jain, S. C., Harker, A. H., Pinardi, K., Willander, M. and Mertens, R. P., Proceedings of the 25th European Solid State Device Research Conference (eds de Graaff, H. C. and van Kranenburg, H.), Editions Frontieres, France, 1995, pp. 459–462.
20. Jain, S. C., Dietrich, B., Richter, H., Atkinson, A. and Harker, A. H., *Phys. Rev.*, 1995, **B52**, 6247–6253.
21. Pinardi, K. and Jain, S. C., unpublished.
22. K. Pinardi, Uma Jain, Jain, S. C., Maes, H. E., Van Overstraeten, R. and Willander, M., *J. Appl. Phys.*, 1998, **83**, 4724–4733.
23. The effect of the finite diameter of laser beam has not been taken into account in these calculations, the peak position $\Delta\omega_{3(\text{eff})}$ can be compared with the experimental values only if there is no variation of stress in the x direction.
24. Olego, D. J., Shahzad, K., Petruzzello, J. and Cammack, D. A., *Phys. Rev.*, 1987, **B36**, 7674.
25. Tu, K.-N., Mayer, J. W. and Feldman, L. C., *Electronic Thin Film Science for Electrical Engineers and Material Scientists*, Maxwell Publishing Co., New York, 1992.
26. *Properties of Silicon*, EMIS Data reviews series no. 4, INSPEC, London, 1988.